ROTOR SLOT PERMEANCE HARMONICS UNDER DISTORTED AIR-GAP FLUX WAVEFORM FOR CAGE INDUCTION MOTOR

Prepared by

S.P. Liou, J.S. Hsu, W.F. Weldon

Presented at

The IEEE Power Engineering Society 1991 Summer Meeting
San Diego, CA

July 28-August 1, 1991

Publication PR-143

Center for Electromechanics
The University of Texas at Austin
Balcones Research Center
Bldg. 133, EME 1.100
Austin, TX 78758
512/471-4496

0216

ROTOR SLOT PERMEANCE HARMONICS UNDER DISTORTED AIR-GAP FLUX WAVEFORM FOR CAGE INDUCTION MOTOR

Shy-Shenq Liou
Member

John S. Hsu
Sr. Member

William F. Weldon
Sr. Member

Center for Electromechanics
The University of Texas at Austin
10100 Burnet Road
Austin, Texas 78758

Design compromise in induction motors sometimes results in significant saturation harmonics. The air-gap flux waveform would be distorted by these saturation harmonics which rotate at exact synchronism with the fundamental flux. A saturated teeth section has flattened air-gap and peaked up core flux waveforms if the core is not saturated. A saturated core and nonsaturated teeth would have a flattened core and peaked up air-gap flux waveforms. If both teeth and core are saturated, numerical field analysis can decide the actual air-gap flux waveform.

Stray losses or stray load losses constitutes a considerable portion of the total losses of an induction motor. The slot harmonics from both stator and rotor, especially from the stator, contribute most to the stray and stray load losses. This paper tries to examine the behaviors of the slot harmonics under distorted air-gap flux waveform. The third-harmonic air-gap flux is intentionally injected into an induction motor to distort the flux waveform. The slot harmonics from the rotor are measured with or without the load under various air-gap flux waveforms including fundamental alone, flattened air gap, and flattened core (peaked up air gap). Test results show that for the tested motor, the air-gap flux waveform (which has lower peak value) would also have lower rotor slot harmonics with or without the load.

Although the stator slot harmonics are not measured directly because of inadequate equipment, the variations of the stator core losses, rotor high frequency losses, and stray load losses (dictated by the stator slot harmonics) suggest that the stator slot harmonics probably behave as the rotor slot harmonics do under distorted air gap flux waveforms. A cageless rotor is used to separate the stator core losses from the no-load losses, which include the stator core losses and the no-load rotor high frequency losses.

ROTOR SLOT PERMEANCE HARMONICS UNDER DISTORTED AIR-GAP FLUX WAVEFORM FOR CAGE INDUCTION MOTOR

Shy-Shenq Liou
Member

John S. Hsu
Sr. Member

William F. Weldon
Sr. Member

Center for Electromechanics
The University of Texas at Austin
10100 Burnet Road, Bldg. 133
Austin, TX 78712

Abstract: The air-gap flux waveform for a cage induction machine is not sinusoidal in shape and contains various harmonics, including the phase-belt harmonics, slot magnetomotive force (mmf) harmonics, slot permeance harmonics, and saturation harmonics. The slot mmf and permeance harmonics affect the stray losses considerably. Among the saturation harmonics, the third harmonic is usually the most significant one unless it is suppressed by allowing circulating current to flow. The magnitude and phase angle of the saturation harmonics compared to those of fundamental flux waveform depend on whether teeth or core (back iron) section is more saturated. The various amount of third harmonic air gap flux with different phase angle is intentionally injected into a cage induction motor to examine the effects of distorted flux waveform on rotor slot permeance harmonics. For the same air gap fundamental flux, the waveform which has the higher air gap peak flux also produce higher rotor slot permeance harmonics. The stator core losses, no-load rotor high frequency losses, no-load losses, and stray load losses under distorted air gap flux waveforms are presented and discussed.

INTRODUCTION

Stray loss (the loss defined as the total loss minus the stator copper loss, stator core loss, rotor fundamental I^2R loss, and friction and windage loss) is a very complicated and important issue for cage induction motor because it constitutes a significant portion of the total loss. The stray loss is different from the stray load loss which is the additional loss caused by the load compared to the no-load loss. The stray loss includes the stray load loss, the no-load rotor high frequency loss, the loss caused by axial end leakage flux, and other miscellaneous losses. The International Electrotechnical Commission (IEC) recommends 0.5% of the output to be the stray load loss for induction motors, and the American National Standards Institute (ANSI) suggests 1.2% for small motors (rating less than 2,500 hp) and 0.9% for large motors. Most designers depend on empirical formula to estimate the stray loss. The understanding of various sources of stray loss would dictate the accuracy of the empirical equations. Extensive literature can be found on this subject [1] with outstanding works reported by Alger [2,3], Christofides [4,5], Chalmers [6,7], and other authors. However the existing literature has not addressed the effect of the distorted air gap flux waveform caused by the saturation on the slot permeance harmonics, which is one of the most significant contributors to the stray or stray load losses [2,3].

It is a well-known fact that saturation of magnetic material can produce significant amount of harmonics [8]. Among the harmonics, the third-harmonic is usually the most dominant one unless circulating current is allowed to cancel all the triplen (triple multiples of the fundamental frequency) harmonics. For rotating machines, design compromise sometimes requires either saturated teeth and/or saturated core. The magnitude and phase angle of saturation harmonics depends on the flux density vs. magnetic intensity (B-H) characteristics of the magnetic material, the degree of saturation on the teeth and core sections, and the winding connection diagram (a delta-connected winding does allow circulating current, for example). The air gap flux distribution of an induction motor can be calculated using the method developed in [9,10] or a finite-element program. If either teeth or core section of induction motor is saturated, the space harmonics caused by saturation are inevitable and they rotate at exact synchronism with the fundamental flux wave. Consequently, the air gap flux waveform is distorted under saturated condition.

Given the facts that the stray losses depend heavily on the slot harmonics and design compromise sometimes calls for saturation harmonics and consequently distorted air gap flux waveform, it is worthwhile examining the effects of distorted air gap flux waveform on slot harmonics. In this paper, the third space harmonic flux is intentionally injected into a cage induction motor to distort the air gap flux waveform. The rotor slot permeance harmonics under distorted air gap flux waveform are examined using the search coils located in the stator slots. Two rotors are used in the tests. One is the normal cage rotor with cast aluminium short-circuited bars and the other rotor has laminated punchings only. To obtain the stator slot harmonics requires either a slip ring and search coils mounted on the rotor or an inverted machine as used in [11]. Unfortunately, neither apparatus is available at this moment, therefore the direct measurement of stator slot permeance harmonics are not performed. However, the stator core losses, no-load rotor high frequency losses, no-load losses, and stray load losses under distorted waveforms are presented. The distorted air gap flux waveforms do affect the no-load rotor high frequency losses and stray load losses which depend heavily on stator slot mmf and permeance harmonics. This result suggests that the stator slot harmonics are affected by the distorted air gap flux waveforms too.

TEST SET-UPS

The tested motor is a Dayton three phase, four pole, 5 hp farm duty cage induction motor, Model No. 3N339B. It contains 36 stator slots and 48 skewed rotor bars. The original windings were striped and a new set of windings is put in to accommodate a combined three phase, six pole fundamental and a two phase, 18-pole third-harmonic excitation. The 60-Hz excitation is from a three-phase autotransformer connected directly to the system and the 180 Hz excitation is from a two channel Crown PSA-1 power amplifier with sinusoidal outputs. The detailed description of the circuit diagram used for the experimental motor can be found in [12,13].

Two three phase digital power analyzers from Valhalla Scientific Model No. 2300 with accuracy of ± 0.25% of reading are used to measure the true root mean square (rms) voltage, current, and actual wattage for each coil of tested induction motors. A strain gauge torque sensor from Eaton Corporation, Model No. 1104-1K is used to measure the output shaft torque from the cage induction motor with a resolution of 0.4 lb-in. A Baldor 7505 dc machine is used to drive the tested motor at 1,200 rpm at no-load and it is also used as a dynamometer for load tests. A Hewlett Packard 3582A spectrum analyzer is used to measure the harmonic content from the air gap search coil which consists of three full pitch, single-turn coils (one from each pole-pair) connected in series. These air gap search coils are located on top of the slot under the insulation wedges. Two additional search coils are also placed in the stator to pick up the teeth and core flux waveforms. The hot resistance of each coil is measured with a Hewlett Packard 3478A digital multimeter with a resolution better than 0.001 Ω right after each test point to ensure that the stator copper loss can be determined accurately.

AIR-GAP AND CORE FLUX WAVEFORMS

The magnitude and phase angle of saturation harmonics in the air gap depend upon the saturation degree of the teeth and/or core section of cage induction machines [10]. If the teeth section is saturated and core is not, the air gap flux waveform would be flattened with a peaked up core flux waveform. If only the core section is saturated, the core flux waveform is flattened with a peaked up air gap flux waveform. This is because the core flux is the integration of air gap flux. The integration process not only changes the relative phase angle between fundamental and third-harmonic fluxes (from flattened to peaked up or vice versa), it also modifies the relative magnitude of third-harmonic flux with respect to the fundamental flux. Since the pole area for the third-harmonic flux is only one-third of that for the fundamental, the ratio of third-harmonic flux and fundamental flux in the core section would be one-third of that in the air gap section. If both teeth and core are saturated, the saturation harmonics from teeth and core would cancel each other at least partially and a detailed field numerical analysis can decide the magnitude and relative phase angle of saturation harmonics with respect to the fundamental flux [14].

Fig. 1 shows three air gap and core flux waveforms for three different cases. Fig. 1(a) is for the fundamental excitation alone. Fig. 1(b) is for fundamental excitation with 12% air gap third-harmonic flux (a flattened air gap flux waveform associated with a peaked up core flux waveform) and is defined as flattened air gap case. Fig. 1(c) is for fundamental excitation with 11% core third-harmonic flux (a flattened core flux waveform with a peaked up air gap flux waveform) and is defined as the flattened core case. The air gap third-harmonic flux in Fig. 1(c) is 33% compared to fundamental air gap flux. In Fig. 1(b), a 12% air gap third-harmonic flux corresponds to a 4% third-harmonic flux in the core section. The percentage chosen for Fig. 1(b) and 1(c) are deemed broad enough to cover most saturated teeth or core conditions for actual punching design. In Fig. 1, the voltage waveform from the air gap full pitch search coil is the air gap flux waveform. The voltage waveform from the core search coil is connected to a passive integrator to yield the core flux waveform. The coordinate dimension in Fig. 1 is for air gap flux waveform only. Peak fundamental air gap flux waveform of 1 T results in 1.17 T peak fundamental core flux waveform.

STATOR CORE LOSS

The no-load test conducted using the normal cage rotor does not yield the actual stator core loss because the power input to the motor minus the stator copper loss at no-load still contains the rotor high frequency losses

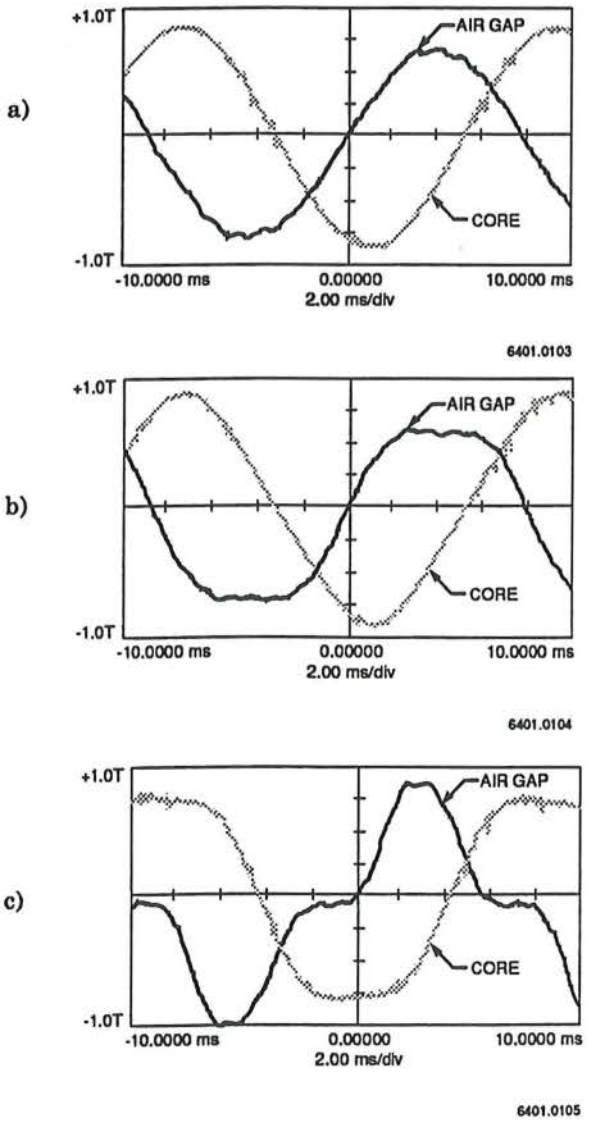

Fig. 1. Air gap and core flux waveforms for a) fundamental alone, b) flattened air gap and c) flattened core

contributed by the stator slot (mmf and permeance) harmonics, and phase-belt harmonics. These high frequency losses constitute a considerable portion of the no-load losses. To obtain a more accurate stator core loss, a rotor which has no cast aluminium short-circuited bars is used in the stator core loss test. Fig. 2 shows this cageless rotor and the normal cage rotor. The difference in outside diameter between these two rotors is 0.005 cm. The shape and the approximate dimension of the rotor slot are shown in Fig. 3. It is quite common for this size of motor to have a narrow bridge on top of the rotor slot and it is expected that a sizable load current flowing in the rotor bar would saturate the bridge. The dc machine is used as a dc motor to drive the cageless rotor at 1,200 rpm during the stator core loss test. The stator core loss P_{score} can be obtained from

$$P_{score} = P1_{in} - P_{scopper} \quad (1)$$

where

$P1_{in}$ = input power
$P_{scopper}$ = stator copper loss

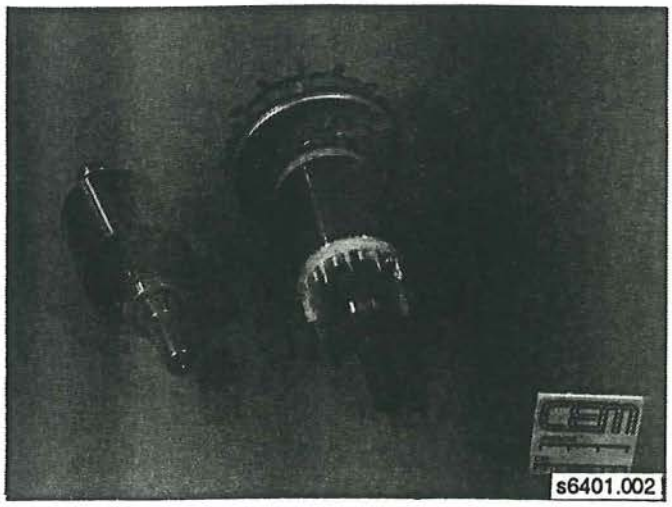

Figure 2. Cage and cageless rotors

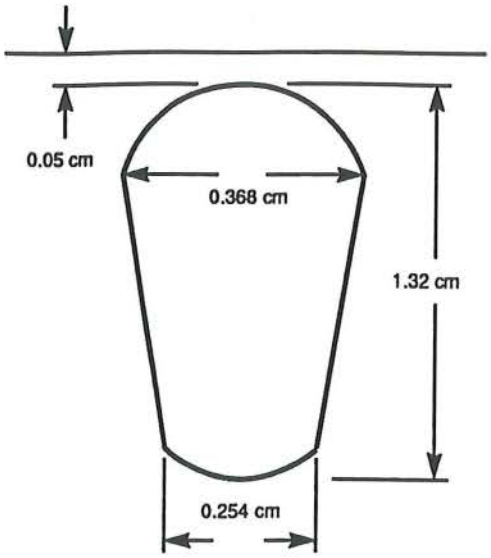

Figure 3. Approximate dimension for rotor slot

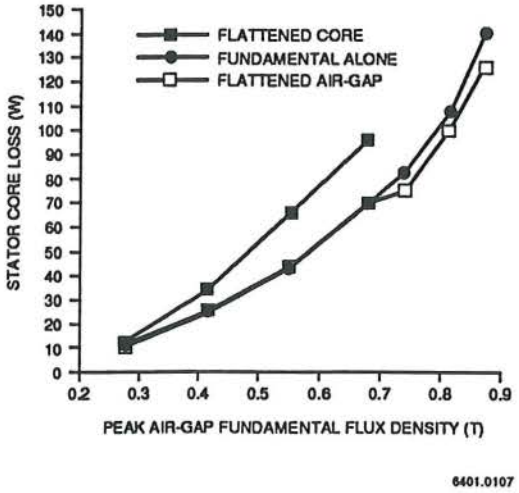

Figure 4. Stator core loss vs. peak air gap fundamental flux density

Since no physical conductors reside inside the rotor, it is assumed that there is no energy conversion across the air gap of the cageless motor. Thus, (1) represents the stator core loss. The stator core losses vs. the fundamental air gap flux density for the cases of fundamental alone, flattened core, and flattened air gap are shown in Fig. 4. It can be seen from Fig. 4 that for the tested motor, the flattened core case has higher stator core loss than those of fundamental alone and flattened air gap cases. This is expected since considerable amount of air gap third-harmonic flux is injected to flatten the core flux waveform, 33% compared to fundamental air gap flux to be exact. Compared to fundamental excitation alone, flattened air gap case has slightly higher (almost indistinguishable) core loss at nonsaturated region and has lower core loss at saturated region. This is because for this specific motor, the teeth would saturate before the core does. Under saturated condition, even the flattened air gap flux waveform is associated with the peaked up core flux waveform (Fig. 1(b)), the saving of core loss in the teeth sections by having lower peak flux waveform does compensate the additional loss incurred in the core section caused by a higher peak flux waveform. In nonsaturated region, the saving from teeth section is slightly smaller than the increased core loss in core section, thus the flattened air gap case has slightly higher stator core loss than the fundamental alone case. The highest percentage reduction in core loss for the tested motor is about 10% at 0.87 T peak air gap fundamental flux density which corresponds roughly to 1.02 T core fundamental flux density and 1.74 T teeth fundamental flux density.

HYSTERESIS TORQUE

The stator core loss P_{score} in (1) excludes the hysteresis power P_{hys} at synchronous speed as explained in [6]. The hysteresis torque tends to drive the rotor in synchronism with the rotating magnetic field, and the input power from the stator contains a corresponding hysteresis torque component. When the slip changes sign from

positive to negative, the stator input power is abruptly reduced by twice the hysteresis power, and the shaft input power from the dc motor is increased by the same amount. A slip test is conducted for fundamental excitation alone at 0.55 T peak air gap fundamental flux density. The electrical input power to cageless induction motor (stator copper loss is excluded) and shaft input power from dc machine vs. the rotor rotating speed are shown in Fig. 5. The hysteresis power P_{hys} is determined from Fig. 5 to be about 13 W. Fig. 5 can also be used to obtain the stator core loss. The 39.9 W from Fig. 5 is fairly close to 42 W from Fig. 4 at 0.55 T peak air gap fundamental flux density.

Slip tests are also conducted for other air gap flux densities. The hysteresis power maintains fairly constant for different air gap flux density. The stator core losses from the slip tests are very close to the values from Fig. 4. Therefore, it is concluded earlier that the stator core loss P_{score} in (1) does not include the hysteresis power P_{hys}.

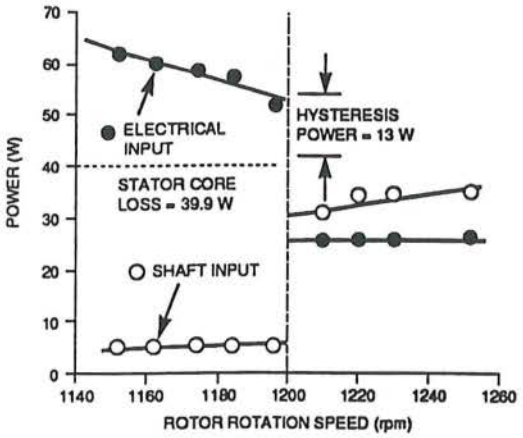

Figure 5. Electrical and shaft power input vs. rotor speed

NO-LOAD ROTOR HIGH FREQUENCY LOSSES

No-load tests are also conducted for the cage rotor while running with the dc machine uncoupled. The rotor high frequency losses $P_{r,hf}$ at no load can be obtained from

$$P_{r,hf} = P2_{in} - P_{scopper} - P_{hys} - P_{fw} - P_{score} \quad (2)$$

$$P_{noload} = P2_{in} - P_{scopper} - P_{hys} - P_{fw} = P_{r,hf} + P_{score}$$

where

$P2_{in}$ = input power
$P_{scopper}$ = stator copper loss
P_{hys} = hysteresis power from Fig. 5
P_{fw} = friction and windage loss (5.6 W)
P_{score} = stator core loss from Fig. 4

The no-load power loss P_{noload} equals the summation of stator core loss P_{score} and the rotor high frequency loss $P_{r,hf}$. Notice that P_{noload} in (2) does not contain the hysteresis power P_{hys} which is usually included in the conventional no-load loss. The no-load fundamental I^2R loss in rotor is neglected since the slip at no load is extremely small (0.08%). Therefore, the no-load rotor high frequency losses can also be called no-load stray losses and it is shown in Fig. 6 vs. the peak air gap fundamental flux density for all three cases. Although the cage rotor is skewed by one rotor slot and the cageless rotor is straight, Fig. 6 still provides a very good indication of the effects of the slot harmonics under different air gap flux waveforms because it is the stator slot mmf and permeance harmonics which contribute most to the rotor high frequency losses at no load [2,3]. Flattened core case has the highest whereas flattened air gap has the lowest no-load rotor high frequency losses in Fig. 6. It can be seen from the figures 4 and 6 that the no-load rotor high frequency losses is sometimes almost as big as the stator core losses for the same fundamental air gap flux density.

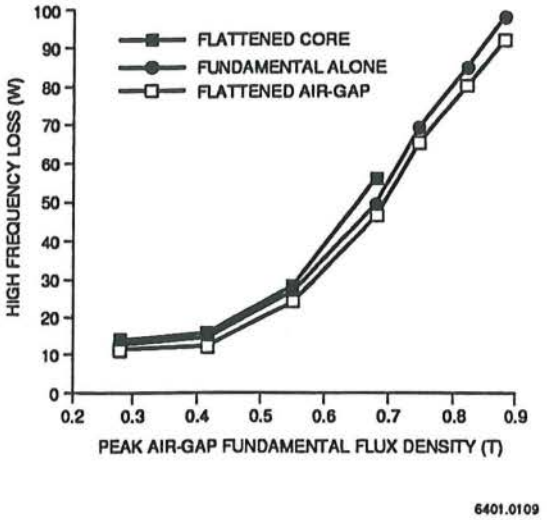

Figure 6. No-load rotor high frequency losses vs. peak air gap fundamental flux density

ROTOR SLOT PERMEANCE HARMONICS

The rotor slot permeance harmonics can be measured directly from the air gap and/or teeth search coils which are located on the stator slots. From [2], the order of rotor slot permeance harmonics n

$$n = \frac{R}{P} \pm 1 \quad (3)$$

where

R = number of rotor bars
P = number of pole pairs

For the tested motor, R = 48 and P = 3. Thus the harmonic orders are 15th and 17th which correspond to 900 and 1,020 Hz respectively at 1,200 rpm. The magnitude of the 15th and 17th harmonics vs.the peak air gap fundamental flux density for the cageless rotor are shown in Fig. 7(a) and (b) respectively. The air gap flux waveforms and the voltage waveforms of teeth search coil for 0.55 T peak air gap fundamental flux density are shown in Fig. 8(a), 8(b), and 8(c) for fundamental alone, flattened air gap, and flattened core cases respectively. From Fig. 7, it can be seen that the flattened core case, having the highest peak air gap flux density (0.55 T × 1.33 = 0.66 T), has the highest rotor slot permeance harmonics. For flattened air gap case, the lowest peak air gap flux density (0.55 T × 0.88 = 0.48 T) produces the smallest rotor slot permeance harmonics. Therefore, the shape of air gap flux waveform does have

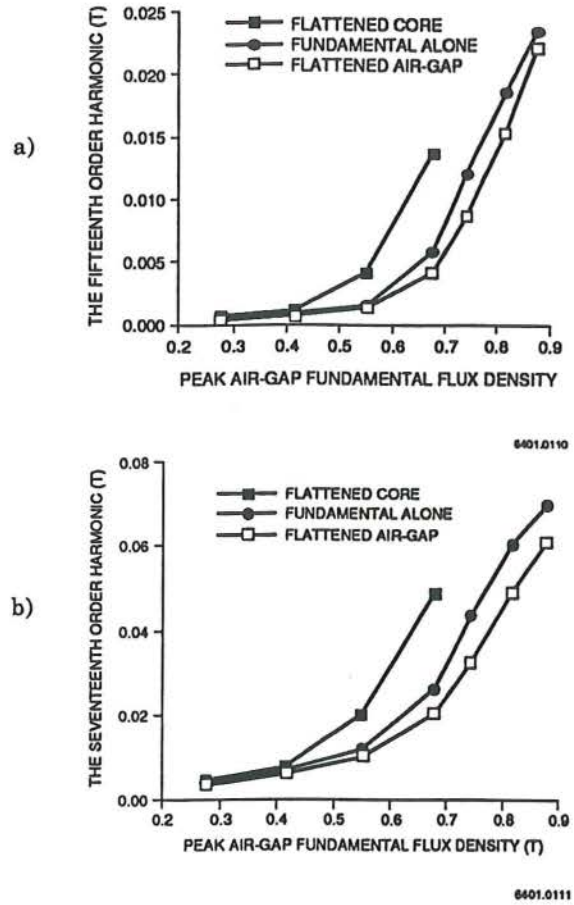

Fig. 7. Rotor slot permeance harmonics for cageless rotor
a) 15th harmonic b) 17th harmonic

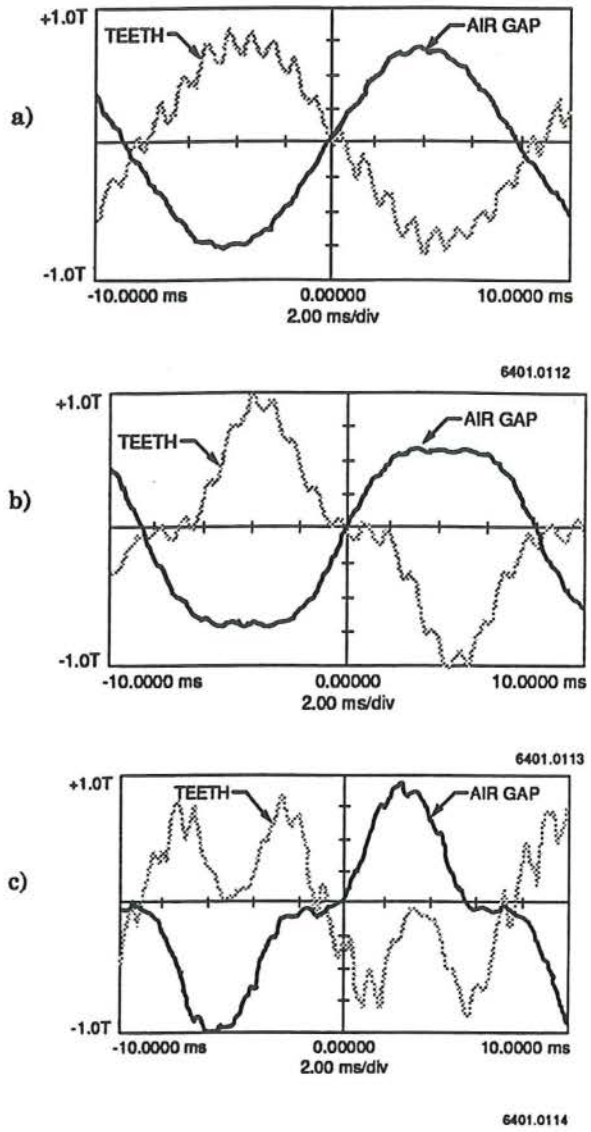

Fig. 8. Air gap flux and teeth voltage waveforms for
a) fundamental alone, b) flattened air gap, and
c) flattened core

significant impact on the rotor slot permeance harmonics. The higher the peak air gap flux density, the higher the permeance harmonics would be. Another point worth noticing is that the magnitude of 15th and 17th harmonics are not the same for all three cases with 17th harmonic being almost three times as big as the 15th harmonics. From [2], the (R+P)/P or 17th harmonic is forward and the (R-P)/P or 15th harmonic is backward rotating fields with respect to the rotor. It is expected that the theory of forward and backward travelling waves used to explain how single phase induction motor works might be used to explain the difference in magnitude between 15th and 17th harmonics.

Same observation can be made by examining Fig. 8 in which the frequency of the perturbations on the teeth voltage waveforms can be determined to be around 1000 Hz and the magnitude of perturbation in Fig. 8(b) and 8(c) are the lowest and highest respectively.

The normal cage rotor which is skewed by about one rotor slot is used in the load test. Fig. 9(a) shows the air gap flux and teeth voltage waveforms for the case of fundamental alone at 0.1 hp load whereas Fig. 9(b) shows the corresponding waveforms for 2.0 hp load. Fig. 9 clearly displays the increased distortion in the air gap flux and teeth voltage waveforms because of load. This phenomenon results from the increased rotor equivalent slot openings because of the saturation of the narrow bridge on top of the rotor slot (Fig. 3) caused by load current in the rotor bars. The rotor slot permeance harmonics under loaded condition for fundamental alone, flattened air gap, and flattened core cases are shown in Fig. 10. The peak air gap fundamental flux density for figures 9 and 10 is 0.55 T. Because the frequency of rotor slot harmonics depends on the rotation speed of the rotor, the measured frequency for 15th and 17th harmonics change from 900 and 1020 Hz (at 0.1 hp) to 864 and 984 Hz (at 2.0 hp) respectively. The rotor speed for 2 hp load is 1,156 rpm for all cases.

Several observations can be made from Fig. 10. First of all, the rotor slot harmonics which includes mmf and permeance harmonics go up with the load. Second, the flattened core case and flattened air gap case still has the highest and lowest harmonics contents respectively. Third (for the same load increase from 0.1 to 2.0 hp) the increase in rotor slot harmonics is smallest for the flattened core case. The increase is about the same for fundamental alone and flattened air gap cases. It is believed that for flattened core case, the equivalent rotor slot opening is bigger than the other two cases at 0.1 hp load. Thus, the additional slot opening caused by the load current should be smaller than the other cases.

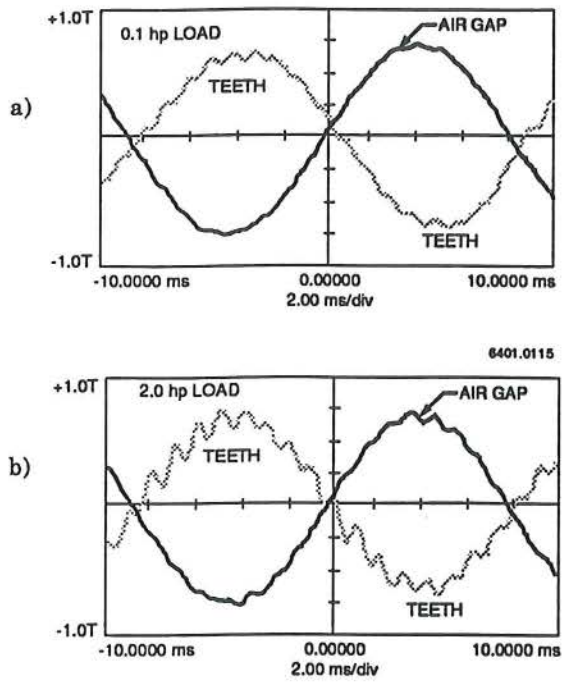

Fig. 9. Air gap flux and teeth voltage waveforms for fundamental alone case
a) at 0.1 hp load and b) at 2.0 hp load

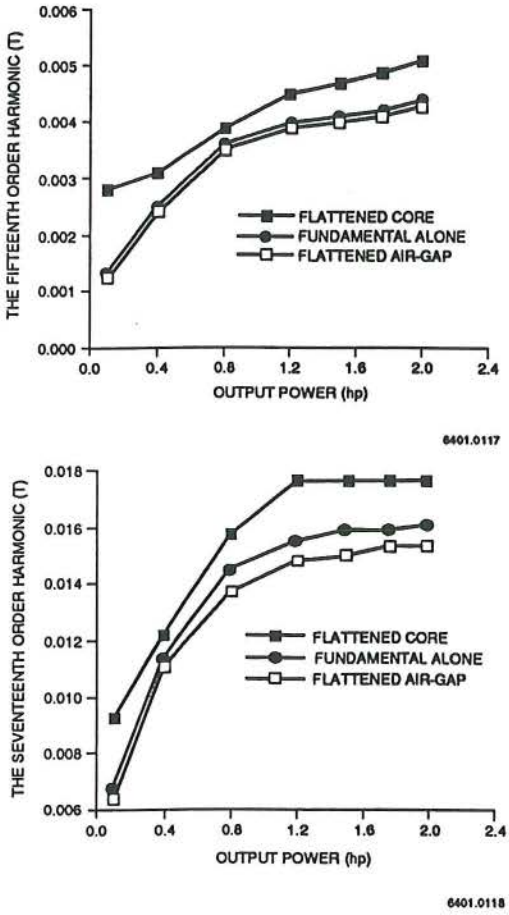

Fig. 10. Rotor slot harmonics under load
a) 15th harmonic and b) 17th harmonic

This argument is furthered enhanced by examining Fig. 11 in which the stray load losses $P_{strayload}$ for those three cases are displayed. The stray load loss $P_{strayload}$ is defined as

$$P_{strayload} = P3_{in} - P_{out} - P_{scopper} - P_{hys} - P_{fw} - P_{noload} - P_{out} \times \frac{s}{1-s} \quad (4)$$

where

$P3_{in}$ = input power
P_{out} = output power
$P_{scopper}$ = stator copper loss
P_{hys} = hysteresis power
P_{fw} = friction and windage loss
P_{noload} = no-load loss as calculated in (2)
s = slip
$P_{out} \times s/1-s$ = rotor fundamental I^2R loss

The flattened core case in Fig. 11 has the lowest stray load loss. This result is not surprising because the degree of saturation is relatively high for flattened core case (air gap peak flux density is increased by 33%) and the stray load losses tend to decrease with increased saturation as indicated in [15]. For flattened air gap case, the degree of saturation is about the same as the fundamental alone case because a 12% reduction in the air gap peak flux density comes with a 4% increase in core flux density (Fig. 1). The lower stray load loss for flattened air gap case compared to the fundamental alone case is expected to result from the lower slot harmonics. Further efforts to measure the stator slot harmonics using search coils on rotor is needed before a firm conclusion can be drawn on the effects of distorted air gap waveforms on the stator slot harmonics, although the stray load losses for flattened air gap case (Fig. 11) is smaller than the stray load loss of fundamental alone case.

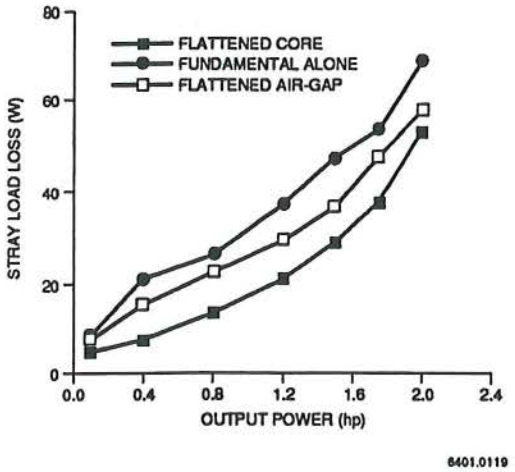

Fig. 11. Stray load losses vs. output power

For the tested motor, since the flattened core case has the highest stator core and no-load losses (Fig. 4), even it has the lowest stray load losses, the total loss it requires to produce the same output is still the highest among all cases studied. The output power versus the total losses curves are shown in Fig. 12.

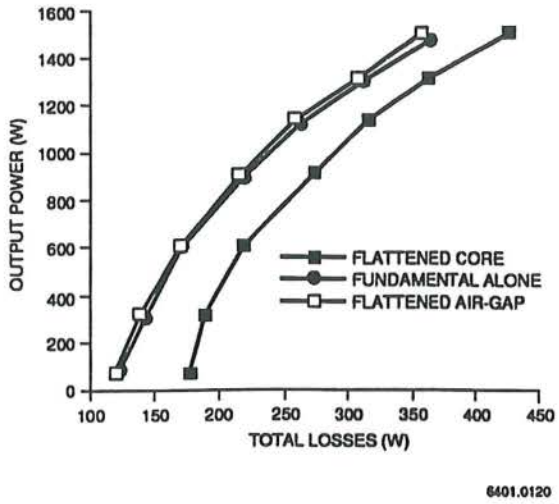

Fig. 12. Output power vs. total losses

DISCUSSION

This paper tries to examines both stator and rotor slot harmonics and their effects on stray and stray load losses under distorted air gap flux waveforms. Although the slot harmonics from rotor is presented, the stator slot harmonics are not measured and reported in this paper because of inadequate equipment, the no-load rotor high frequency losses and stray load losses (which are the losses heavily affected by the stator slot harmonics) does show that they have a close correlation with the distorted air gap flux waveforms. As can be seen from Figs. 2 and 3, the tested rotor has closed slots which are far different from the open or semiclosed stator slots used commonly for most cage induction motors. It is expected that the effects of distorted air gap flux waveforms on these open or semiclosed stator slots (which have relative big air gaps between the tips of the teeth) might be smaller compared to their effects upon closed slots like the one used in the tests.

On the other hand, the results from this paper might be more pertinent to the machines with magnetic wedges on the stator [16]. After all, slots with magnetic wedges are very similar to the closed slots if the wedges are not saturated. Under this condition, different air gap flux waveforms might cause sizable difference in stator slot harmonics.

CONCLUSIONS

The distorted air gap flux waveforms have considerable impact on the rotor slot permeance harmonics under no-load and loaded conditions. A saturated core and nonsaturated teeth result in flattened core and peaked up air gap flux waveforms. The rotor slot permeance harmonics would also be higher. A saturated teeth and nonsaturated core would produce flattened air gap and peaked up core flux waveforms and lower rotor slot permeance harmonics.

If the teeth section is easier to saturate than the core section, third-harmonic flux can be used to flattened the air gap flux waveform and to reduce the stator core loss, no-load rotor high frequency loss, no-load losses, and stray load loss. The highest percentage reduction for stator core loss for the tested motor is 10% when the teeth section is saturated. For the same reason, if core section is easier to saturate than the teeth section, third-harmonic flux can be used to flatten the core flux waveform to reduce the no-load loss as reported in [15].

Based on the no-load rotor high frequency losses and stray load losses reported in this paper, the stator slot harmonics which affect the stray losses of cage induction motor most are expected to behave as the rotor slot harmonics do under distorted air gap flux waveforms.

No-load rotor high frequency loss constitutes a significant portion (up to 45% for the tested motor) of the conventional no-load loss which is taken as the power input minus the stator copper loss while the motor is running without any load.

The magnitude of the principle rotor slot permeance harmonics is not the same based on air gap search coil measurement. For the tested motor, the 17th harmonic is almost three time as big as the 15th harmonic.

ACKNOWLEDGMENTS

The authors would like to thank the State of Texas for financial support through a grant under Texas Advanced Technology Program, Grant No. 1591 and 003658-181. National Science Foundation also provides financial assistance through Grant No. ECS-880884 which is deeply appreciated. The authors are indebted to Mr. Jerry Lloyd of Emerson Electric Company for providing the cageless rotors. Special thanks are given to supporting staff of the Center for Electromechanics, The University of Texas at Austin for their assistance during the course of this study and in preparing this paper.

REFERENCES

[1] Jimoh, A.A., Findlay, R.D., and Poloujadoff, M., "Stray Losses in Induction Machines, Part I and II,"*IEEE Transactions on Power Apparatus and System*, Vol. 104, No. 7, June 1985, pp. 1500-1512.

[2] Alger, P.L., *The Nature of Induction Machines*, Gordon and Breach, New York, 1965.

[3] Alger, P.L., Angst, G., Davies, E.J., "Stray-Load Losses in Polyphase Induction Machines," *AIEE Transactions*, Vol. 78, June 1959, pp. 349-357.

[4] Christofides, N., "Origins of Load Losses in Induction Motors with Cast Aluminium Rotors," *IEE Proceedings*, Vol. 112, No. 12, 1965, pp. 2317-2332.

[5] Christofides, N., "Determination of Load Losses and Torques in Squirrel-Cage Induction Motors", *IEE Proceedings*, Vol. 113, No. 12, 1966, pp. 1995-2005.

[6] Chalmers, B.J., Richardson, J., "Investigation of High-Frequency No-load Losses in Induction Motors with Open Stator Slots," *IEE Proceedings*, Vol. 113, No. 10, 1966, pp. 1597-1605.

[7] Chalmers, B.J., Chandra, K.N., "High-Frequency No-Load Losses of Cage Induction Motors," *IEEE Transactions on Power Apparatus and Systems*, Vol. 89, No. 6, 1970, pp. 1043-1049.

[8] Hsu, John S., Woodson, Herbert H., and Liou, Shy-Shenq P., "Experimental Study of Harmonic-Flux Effects in Ferromagnetic Materials," *IEEE Transactions on Magnetics*, Vol. 25, No.3, page 2678-2685, May, 1989.

[9] Chalmers, B.J., Dodgson, R., "Waveshapes of Flux Density in Polyphase Induction Motors under Saturated Conditions," *IEEE Transactions on Power Apparatus and Systems*, Vol. 90, No. 2, 1971, pp. 564-569.

[10] Cistelecan, M., Onica, P., "New Improvements in the Computation of the Polyphase Induction Motor Magnetic Circuit," *IEE Proceedings*, Vol. 123, No. 4, 1976, pp. 335-341.

[11] Chalmers, B.J., Sarkar, B.R., "High Frequency Effects in Induction Motors," *IEE Proceedings*, Vol. 114, No. 10, 1967, pp. 1518-1519.

[12] Liou, Shy-Shenq P., Herbert H. Woodson, Hsu, John S., "Steady-State Performance of Reluctance Motors under Combined Fundamental and Third-Harmonic Excitation, Part I: Theoretical Analysis," Paper Submitted to IEEE Power Engineering Society 1991 Summer Meeting.

[13] Liou, Shy-Shenq P., Herbert H. Woodson, Hsu, John S., "Steady-State Performance of Reluctance Motors under Combined Fundamental and Third-Harmonic Excitation, Part II: Experimental Results," Paper Accepted for presentation at IEEE Power Engineering Society 1991 Winter Meeting, New York.

[14] Fuchs, E.F., Chang, L.H., Appelbaum, J., "Magnetizing Current, Iron Losses and Forces of Three-Phase Induction Machines at Sinusoidal and Nonsinusoidal Terminal Voltage, Part I and II,", *IEEE Transactions on Power Apparatus and Systems*, Vol. 103, No. 11, 1984, pp. 3303-3325.

[15] Hsu, John S., Liou, Shy-Shenq P., B.T. Lin, and W.F. Weldon, "Losses Influenced by Third-Harmonic Flux in Induction Motors," Paper Accepted for presentation at IEEE Power Engineering Society 1991 Winter Meeting, New York.

[16] Akio Kaga, Yoshihisa Anazawa, and Hideo Akagami, "The Efficiency Improvement of Capacitor Motor with Ferrite Magnetic Wedges," *IEEE Transactions on Magnetics*, Vol. 22, No.5, page 964-966, May, 1986.

[17] Spooner, E., "Stray Loss in Solid-Rotor Induction Machines," *IEE Proceedings*, Vol. 129, Part B, No. 4, 1982, pp. 181-189.

BIBLIOGRAPHY

Shy-Shenq P. Liou (M '89) was born in Taiwan, Republic of China and received a BSEE degree from the National Taiwan University in 1981. After nearly two years service in the Chinese Air Force, he entered The University of Texas at Austin in 1983 and earned MSEE and PhD degrees in electrical and computer engineering from the same university in 1985 and 1989 respectively. At present, he is conducting research in the area of rotating machines and power electronics as a research engineering associate in the Center for Electromechanics, The University of Texas at Austin. Dr. Liou is a member of Tau Beta Pi.

John S. Hsu (or Htsui) (SM '89) was born in China. He received a BS degree from Tsing-Hua University, Beijing, China, and a PhD degree from Bristol University, England, in 1959 and 1969, respectively. He joined the Electrical and Electronics Engineering Department of Bradford University, England, serving there nearly two years.

After his arrival in the United States in 1971, he worked in research and development areas for Emerson Electric Company and later for Westinghouse Electric Corporation. Presently he is manager of the Industrial Drives Program, Center for Electromechanics, The University of Texas at Austin. Dr. Hsu is a chartered engineer in the United Kingdom and a registered professional engineer in Texas, Missouri, and New York.

William F. Weldon earned his BSES from the Trinity University, San Antonio in 1967 and MSME from The University of Texas at Austin in 1970. At The University of Texas at Austin, he was appointed Jack S. Josey Professor in Energy Studies in 1990, Director of the Center for Fusion Engineering in August 1988, Professor of Electrical and Computer Engineering and Mechanical Engineering in 1986, and Director of the Center for Electromechanics (CEM) in 1985. Prior to that, he served at Technical Director of CEM since its establishment in 1977 and as chief Engineer of CEM's Predecessor, the Energy Storage Group, from 1973 to 1977. Professor Weldon has served on over 19 advisory panels and committees and has seven years of professional experience in industry where he was engaged in the design and development of mechanical and electromechanical prototypes. A registered professional engineer in Texas he has been a consultant to more than 20 groups or firms since 1974, including American as well as European firms. He has authored over 271 technical publications, and holds 21 patents in the area of rotating electrical machinery and pulsed power with six patents pending.